


Determination of the top-quark mass from top-quark pair events with the matrix element method at next-to-leading order: Potential and prospects

Till Martini^{*}*Fraunhofer Zentrum SIRIOS, Fraunhofer Institute for High-Speed Dynamics EMI, Berlin, Germany*Turan Nuraliyev[†] and Peter Uwer[‡]*Humboldt-Universität zu Berlin, Institut für Physik, Newtonstraße 15, 12489 Berlin, Germany* (Received 18 January 2023; accepted 22 March 2023; published 19 April 2023)

In 2004 the matrix element method was used in a pioneering work by the Tevatron experiment $D\bar{0}$ to determine the top-quark mass from a handful of events. Since then the method has matured into a powerful analysis tool. While the first applications were restricted to leading-order accuracy, the extension to next-to-leading order (NLO) accuracy has also been studied. In this article we explore the potential of the matrix element method at NLO to determine the top-quark mass using events with pair-produced top quarks. We simulate a toy experiment by generating unweighted events with a fixed input mass and apply the matrix element method to construct an estimator for the top-quark mass. Two different setups are investigated; unweighted events obtained from the fixed-order cross section at NLO accuracy as well as events obtained using POWHEG matched to a parton shower. The latter lead to a more realistic simulation and allow to study the impact of higher-order corrections as well as the robustness of the approach. We find that the matrix element method in NLO accuracy leads to a significant reduction of the theoretical uncertainties compared to leading order. In view of the high-luminosity phase of the LHC, this observation is especially relevant in analyses which are no longer dominated by statistical uncertainties.

DOI: [10.1103/PhysRevD.107.076013](https://doi.org/10.1103/PhysRevD.107.076013)

I. INTRODUCTION

Regarding experimental as well as theoretical progress, hadronic top-quark pair production has evolved into one of the flagship processes at the LHC. This development is propelled by the expectation of the top quark to play a prominent role in extensions of the Standard Model due to it being by far the heaviest of the elementary particles with a lifetime significantly shorter than the time scale of hadronization. The high production rate of top-quark pairs at the LHC as well as onward advances in experimental data taking enable for ever-decreasing statistical and systematic uncertainties in the recorded data. In order to make optimal use of this fact in experimental analyses, the

employed theoretical predictions are required to keep up in terms of uncertainties.

The next-to-leading order QCD corrections for top-quark pair production have been calculated for the spin-independent case more than 30 years ago [1–4]. Later, also the spin-dependent cross sections were evaluated at NLO accuracy in QCD [5,6]. In a series of ground breaking articles also the next-to-next-to-leading order QCD corrections were calculated [7–11]. Furthermore, beyond fixed order also the resummation of soft-gluon corrections has been studied in great detail ([12–19]). In addition to QCD corrections also weak and QED corrections have been calculated [20–24]. In summary, many detailed theoretical predictions for top-quark pair production are available. However, these might not be readily applicable in the experimental analysis. It is thus important to put more effort in improving the interface between experiment and theory to make optimal use of the increasing precision reached in both fields.

Multivariate analysis methods like the matrix element method (MEM), turn out to be particularly useful in making optimal use of the theoretical predictions. The MEM requires the calculation of event weights in terms of differential cross sections and is thus often formulated at lower-order accuracy only. At leading order (LO), the

^{*}Work on this article was conducted while employed at Humboldt-Universität zu Berlin, Institut für Physik, Berlin, Germany. Till.Martini@physik.hu-berlin.de

[†]Turan.Nuraliyev@physik.hu-berlin.de

[‡]Peter.Uwer@physik.hu-berlin.de

Published by the American Physical Society under the terms of the [Creative Commons Attribution 4.0 International license](https://creativecommons.org/licenses/by/4.0/). Further distribution of this work must maintain attribution to the author(s) and the published article's title, journal citation, and DOI. Funded by SCOAP³.

MEM has been established as a powerful analysis tool for both signal searches as well as parameter inference by virtue of its optimal utilization of the information content of the available data. Typically, the impact of higher-order QCD corrections on theoretical predictions can be significant while often simultaneously decreasing the theoretical uncertainties. In the quest for accuracy and precision to match experimental achievements, the MEM at next-to-leading order (NLO) represents a promising remedy. But when taking higher-order corrections into account, the calculation of event weights constitutes a nontrivial task due to the intricate combination of virtual and real contributions to obtain meaningful finite results. The problem of extending the MEM beyond the Born approximation has been solved in the past by introducing modified jet algorithms on the one hand or sensible event definitions on the other hand ([25–27]). At the same time, the application of the MEM at NLO has been demonstrated for top-quark mass extraction from simulated single top-quark events ([25–27]) as well as anomalous coupling parameter determination from simulated Higgs boson events in association with a single top quark ([28]). Additionally, the effects of a parton shower applied to simulated single top-quark data has been investigated with the MEM at NLO ([27]). In this work, we present the application of the MEM at NLO to top-quark pair production at the LHC. In contrast to the electroweak production mechanism of single top quarks studied before, top-quark pair production is QCD induced at LO already with the two production channels of quark-antiquark annihilation and gluon-gluon fusion constituting the dominant source of top quarks at the LHC. Given the aforementioned prominent role of top-quark pair production in both experimental as well as theoretical advances at the LHC, it represents an ideal example to study higher-order effects within the MEM. Furthermore, in view of the ongoing progress in top-quark mass measurements, the MEM at NLO accuracy could be an interesting alternative to existing approaches.

The paper is structured as follows. In Sec. II the NLO QCD calculation of the differential cross section for top-quark pair production with the phase space slicing method and the subsequent generation of unweighted events are briefly reviewed. Section III focuses on the application of the MEM to the generated events. To study parton shower effects, events generated with POWHEG + Pythia [29–33] are also analyzed. The conclusions are presented in Sec. IV.

II. TOP-QUARK PAIR PRODUCTION AT THE LHC

A. Implementing the NLO prediction with the phase space slicing method

The MEM at NLO as presented in [25–27] requires the cross section calculation at NLO to be carried out using the phase space slicing method [34]. The respective calculation is available in the literature [5]. Thus, in this section we

only give a brief review of the important aspects of the calculation and present the validation for the choice of the slicing parameter. In the phase space slicing method, the cross section prediction at NLO accuracy $d\sigma_{\text{NLO}}$ is formed of two contributions: First, the so-called hard part $d\sigma_{\text{Hard}}$ is just the matrix element for the real corrections evaluated for phase-space points where all partons are resolved, that is the additional parton is neither collinear to the incoming partons nor soft. Second, a Born-like part is comprised of the Born contribution $d\sigma_{\text{LO}}$, the virtual corrections $d\sigma_{\text{virtual}}$ (taken from Ref. [35]) as well as the so-called *soft* and *collinear parts* $d\sigma_{\text{soft/coll}}$ stemming from approximated real corrections integrated over phase-space regions in which the additional parton is unresolved. The separation of the phase space for the real corrections into resolved and unresolved regions is mediated by the so-called slicing parameter x_{min} which acts as a scale to separate the two. In the unresolved regions, well-known factorization properties of QCD real corrections can be employed allowing to analytically integrate over the additional radiation in the singular limits in an approximate way thereby reducing the respective phase space to Born-like kinematics. The divergences of these integrations can be regularized within dimensional regularization leading to poles in the dimensional shift away from four space-time dimensions. The outcome can be combined with the virtual contributions to cancel the respective poles from the loop integration and yield finite results according to the Kinoshita-Lee-Nauenberg theorem [36,37]. Since the real corrections are approximated in the unresolved (singular) regions, the result is only accurate up to deviations proportional to the slicing parameter x_{min} ,

$$d\sigma_{\text{NLO}} = d\sigma_{\text{Hard}} + d\sigma_{\text{LO}} + d\sigma_{\text{virtual}} + d\sigma_{\text{soft/coll}} + \mathcal{O}(x_{\text{min}}). \quad (1)$$

Additionally, the separation of the real phase space in terms of the slicing parameter introduces logarithmic dependencies of the hard and soft/collinear contributions on x_{min} which cancel in the sum. However, when numerically integrating over the finite hard contribution, these logarithms can lead to numerical instabilities if x_{min} is chosen too small. Hence, the value of x_{min} has to be chosen as a compromise between numerical stability and the demand that the deviation in Eq. (1) is negligible compared to the statistical uncertainties of the total cross section as well as distributions calculated at NLO accuracy. Figure 1 shows NLO predictions for the total cross section of top-quark pair production for different values of the slicing parameter x_{min} . The total cross section as the sum of Born, virtual and real contributions in Fig. 1 is indeed finite. However, it shows a systematic deviation from the reference value taken from HATHOR [38] for values $x_{\text{min}} \gtrsim 2 \times 10^{-3}$ while for values $x_{\text{min}} \lesssim 5 \times 10^{-6}$ numerical instabilities dominate. Accordingly, a value of $x_{\text{min}} = 10^{-4}$ is chosen. As an example of a differential distribution the top-quark transverse momentum calculated at NLO accuracy is shown

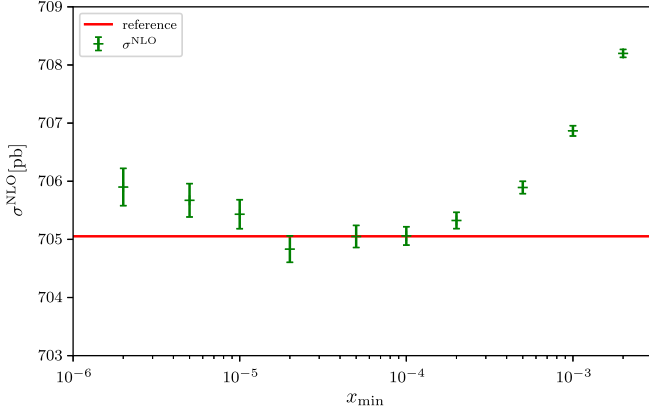


FIG. 1. Phase-space slicing parameter (in-)dependence of the total cross section predicted at NLO accuracy. The red line shows the reference value taken from HATHOR [38].

for three different choices of x_{\min} in Fig. 2. In the lower plot we show for different choices of x_{\min} the differences in units of the statistical uncertainties. We conclude that all three choices lead to coherent predictions justifying the choice $x_{\min} = 10^{-4}$. In addition to the top-quark transverse momentum this has been checked also for the top-quark energy distribution and the rapidity distribution. Furthermore, the distributions calculated here have been cross checked with results from madgraph5 aMC@NLO [39]. The comparison is shown in Appendix, Fig. 9, and Fig. 10. The impact of the NLO corrections on kinematic distributions is displayed in Fig. 3 where NLO and LO predictions for kinematic distributions are compared and their ratios (the k -factor) are shown at the bottom of the plots. Results for further distributions are shown in Fig. 11 in Appendix. As can be seen from the rather constant k -factors, the NLO corrections only mildly affect the shapes of the kinematic distributions. However, the NLO corrections lead to a significant increase of the cross sections by a factor of roughly 1.5. In Fig. 4 the impact of variations of the factorization scale μ_F and renormalization scale μ_R by a factor of 2 as a means to estimate the

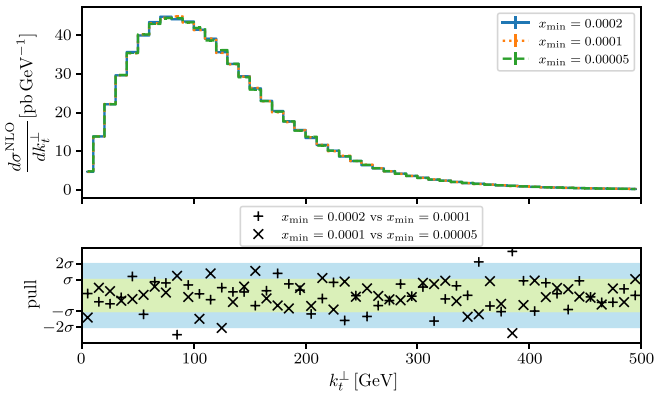


FIG. 2. Phase space slicing parameter (in-)dependence of the top-quark transverse momentum k_T^\perp predicted at NLO accuracy.

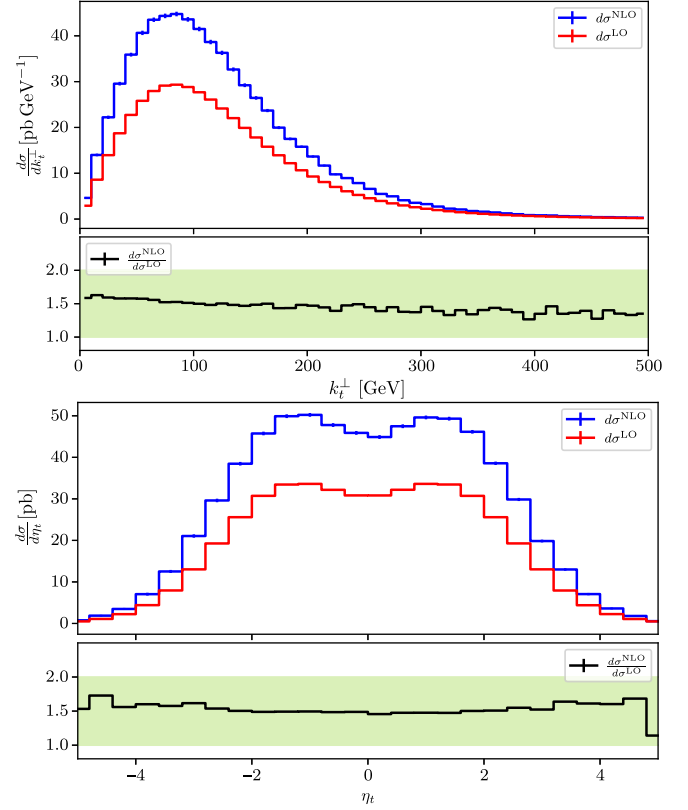


FIG. 3. Differential distributions together with the respective k -factors.

effect of uncalculated higher orders are illustrated for the shapes of two representative kinematic distributions of the top quark. For moderate energy scales, one observes a significant reduction of the impact of the scale variation.

B. Unweighted event generation

From the calculation of the cross section at NLO accuracy outlined in the previous section, event weights can be calculated which can be used to generate unweighted events which are distributed according to the NLO cross section. As described in Ref. [27], a sensible event definition is mandatory for obtaining meaningful event weights at NLO accuracy. In particular, the event definition must not fix the invariant masses or the overall transverse momentum of the final-state objects. For top-quark pair production, we define events \vec{x} in terms of the transverse momentum k_T^\perp , azimuthal angle ϕ_t and pseudorapidity η_t of the top quark as well as the pseudorapidity of the antitop quark $\eta_{\bar{t}}$,

$$\vec{x} = (k_T^\perp, \phi_t, \eta_t, \eta_{\bar{t}}). \quad (2)$$

The two-particle Born phase space as well as the three-particle phase space for the real radiation can be parametrized in terms of these variables

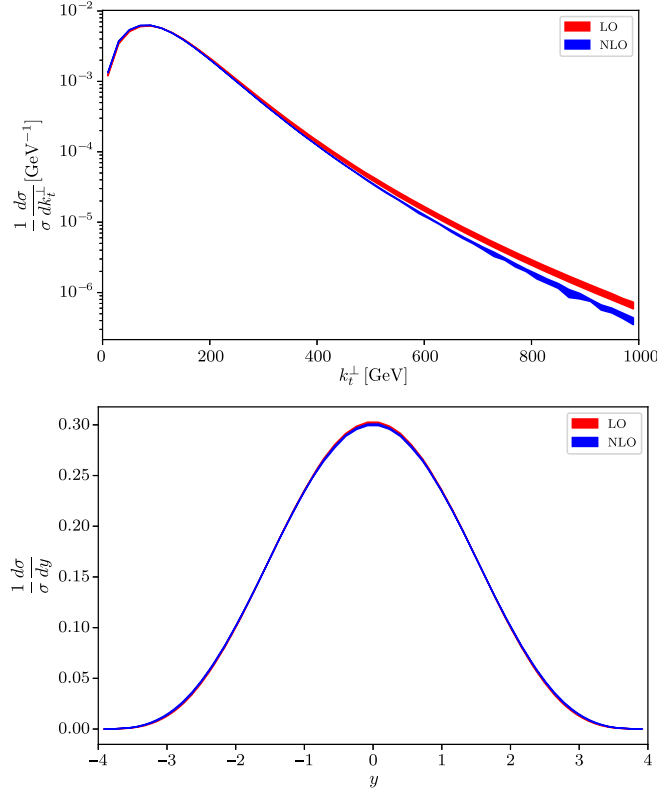


FIG. 4. Effect of scale variations on the shapes of kinematic distributions of the top quark.

$$dR_2 = \frac{k_t^{\perp 3} \cosh \eta_t \cosh \eta_{\bar{t}}}{8\pi^2 E_t E_{\bar{t}} s_{\text{had}}} dk_t^{\perp} d\phi_t d\eta_t d\eta_{\bar{t}}, \quad (3)$$

$$dR_3 = \frac{k_t^{\perp 2} k_{\bar{t}}^{\perp} k_3^{\perp 2} \cosh \eta_t \cosh \eta_{\bar{t}} \cosh \eta_3}{128\pi^5 E_t E_{\bar{t}} E_3 s_{\text{had}}} \times dk_t^{\perp} d\phi_t d\eta_t d\eta_{\bar{t}} dk_3^{\perp} d\phi_3 d\eta_3, \quad (4)$$

where E_i ($i = t, \bar{t}, 3$) denotes the energy of particle i and s_{had} is the hadronic center-of-mass energy squared. The additional radiation occurring in the real corrections is parametrized by the transverse momentum k_3^{\perp} , the azimuthal angle ϕ_3 and the pseudorapidity η_3 of the radiated parton. These parametrizations allow us, together with Eq. (1), to calculate the event weight at NLO accuracy for each event \vec{x} using

$$\begin{aligned} \frac{d^4 \sigma_{\text{NLO}}}{dk_t^{\perp} d\phi_t d\eta_t d\eta_{\bar{t}}} &= \frac{d^4 \sigma_{\text{LO}}}{dk_t^{\perp} d\phi_t d\eta_t d\eta_{\bar{t}}} \\ &+ \int \frac{d^7 \sigma_{\text{Hard}}}{dk_t^{\perp} d\phi_t d\eta_t d\eta_{\bar{t}} dk_3^{\perp} d\phi_3 d\eta_3} dk_3^{\perp} d\phi_3 d\eta_3 \\ &+ \frac{d^4 \sigma_{\text{Virtual}}}{dk_t^{\perp} d\phi_t d\eta_t d\eta_{\bar{t}}} + \frac{d^4 \sigma_{\text{soft/collinear}}}{dk_t^{\perp} d\phi_t d\eta_t d\eta_{\bar{t}}}. \end{aligned} \quad (5)$$

The weights calculated in this way can also be used to generate unweighted events with, e.g., the *von-Neumann*

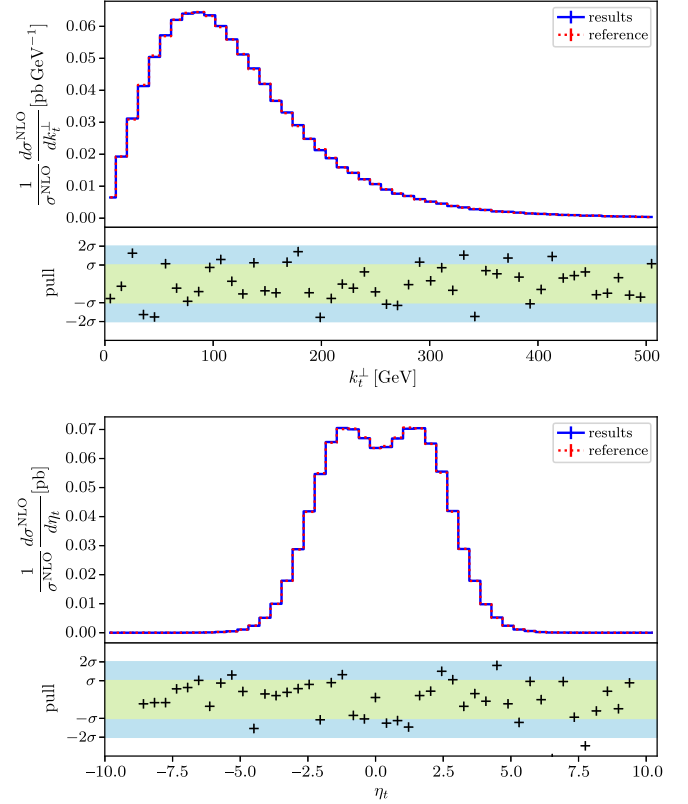


FIG. 5. Validation of the event generation: Comparison of differential distributions of the top quark obtained from unweighted events with results from `madgraph5 aMC@NLO`.

acceptance-rejection method ([40]). Figure 5 shows the distribution of the unweighted events compared to kinematic distributions obtained with the `madgraph5 aMC@NLO` code [39]. The events obtained from the event weights defined in Eq. (5) are within the uncertainties in perfect agreement with the predictions obtained using `madgraph5 aMC@NLO`. In Appendix (Fig. 12) we show in addition the calculation of the $M_{\bar{t}}$ and the ϕ_t -distribution with the same perfect agreement. The comparison of the generated unweighted events with the results from `madgraph5 aMC@NLO` also serves as a further validation for the choice of the slicing parameter.

III. APPLICATION: DETERMINATION OF THE TOP-QUARK MASS USING THE MEM AT NLO

The event weights defined in Eq. (5) can be used in the MEM to calculate the likelihood at NLO accuracy for a given sample of N events $\{\vec{x}_i\}, i = 1, \dots, N$,

$$\mathcal{L}(\{\vec{x}_i\} | m_t) = \frac{1}{(\sigma_{\text{NLO}}(m_t))^N} \prod_{i=1}^N \frac{d^4 \sigma_{\text{NLO}}(m_t)}{dk_t^{\perp} d\phi_t d\eta_t d\eta_{\bar{t}}}|_{\vec{x}=\vec{x}_i}, \quad (6)$$

where the dependence of the total and differential cross sections on the value of the top-quark mass is

highlighted—exemplarily for generic model parameters. Here, the so-called *transfer functions*, parametrizing the probability of measuring a certain signal in the detector given a particular partonic configuration, are set to delta functions. The transfer functions account for particle decays, additional radiation as well as detector effects. Thus, this choice for the transfer functions corresponds to the assumption of a perfect detector which allows a perfect unfolding from the detector signals to partonic variables. While for variables related to angles, setting the transfer function to delta function may give a reasonable approximation, this is not necessarily true in case of variables sensitive to energies. In future applications nontrivial transfer functions should thus be incorporated. This may be done using invertible neural networks trained to a full simulation as discussed in great detail in Ref. [41]. This is however beyond the scope of this work which focuses on exploring the potential of the method for top-quark mass measurements. Maximizing the likelihood with respect to the parameter m_t yields an estimator for the top-quark mass \hat{m}_t ,

$$\mathcal{L}(\{\vec{x}_i\}|\hat{m}_t) = \max_{m_t}(\mathcal{L}(\{\vec{x}_i\}|m_t)). \quad (7)$$

Because the event weights in Eq. (6) are normalized to yield probabilities, the MEM is only sensitive to the shapes of kinematic distributions but not to the total number of events in the sample. To also benefit from the information of the total event number the so-called extended likelihood can be used. The extended likelihood is obtained from the likelihood in Eq. (7) by multiplying with the Poisson probability for observing N events when the expected number of events is given by the total cross section times the integrated luminosity L_{int} of the collider,

$$\mathcal{L}_{\text{ext}}(\{\vec{x}_i\}|m_t) = \frac{(\sigma_{\text{NLO}}(m_t)L_{\text{int}})^N}{N!} e^{-\sigma_{\text{NLO}}(m_t)L_{\text{int}}} \mathcal{L}(\{\vec{x}_i\}|m_t). \quad (8)$$

In Fig. 6 we show the likelihood obtained analyzing 9900 unweighted top-quark pair events distributed according to the NLO prediction. Likelihood (upper plot) as well as the extended likelihood (lower plot) have been studied. The green curves correspond to likelihoods calculated at NLO accuracy using different choices for the factorization and renormalization scale. The orange curves are obtained using only LO predictions again for different scale settings in the likelihood calculation. The analyzed events are generated for an input value of the top-quark mass of $m_{\text{true}} = 173.2$ GeV and the scale choice $\mu_F = \mu_R = \mu_0 = m_t$. The extracted values for the estimator of the top-quark mass together with statistical and systematic uncertainties are summarized in Table I. The estimators \hat{m}_t are determined from the minima of the parabolas fitted to the negative logarithms of the likelihood functions while the statistical uncertainties Δ_{stat} are estimated from their widths. The systematic uncertainties

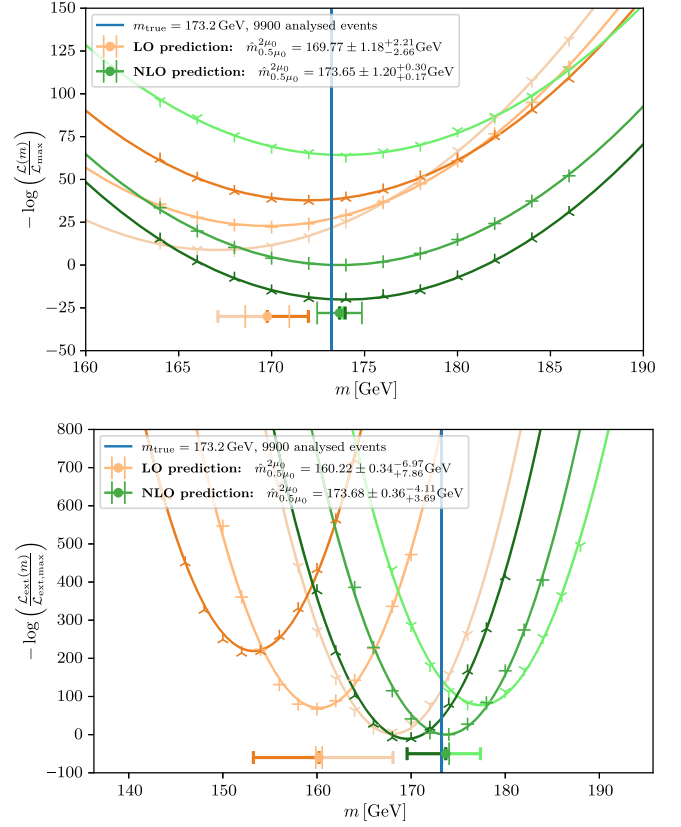


FIG. 6. Analysis of unweighted events following the fixed-order NLO prediction with (extended) likelihoods calculated at LO and NLO accuracy.

$\Delta_{\text{sys}}^{2\mu_0}$, $\Delta_{\text{sys}}^{\mu_0/2}$ are estimated by varying the scale by a factor 2 around μ_0 . As can be seen from Fig. 6 and Table I, both the NLO and the LO analyses have similar statistical uncertainties of about 1.2 GeV and 0.35 GeV depending on whether the likelihood or the extended likelihood is employed. As expected, the statistical uncertainties are to good approximation independent from the perturbative order of the theoretical predictions of the cross sections. Taking the statistical uncertainties into account, the extracted estimators from the NLO analyses are in perfect agreement with the input value. For the likelihood as well as for the extended likelihood the NLO differential cross section matches the probability distribution underlying the event sample thus leading to an unbiased estimator. Obviously, taking into

TABLE I. Extracted values for the estimator of the top-quark mass from 9900 unweighted events following the fixed-order NLO prediction.

	$\hat{m}_t \pm \Delta_{\text{stat}} \Delta_{\text{sys}}^{2\mu_0} \Delta_{\text{sys}}^{\mu_0/2}$ [GeV]	
Likelihood	LO prediction	NLO prediction
\mathcal{L}	$169.77 \pm 1.18^{+2.21}_{-2.66}$	$173.65 \pm 1.20^{+0.30}_{-0.17}$
\mathcal{L}_{ext}	$160.22 \pm 0.34^{+6.97}_{-7.86}$	$173.68 \pm 0.36^{+4.11}_{-3.69}$

account the information on the total number of events via the extended likelihood leads to a reduction of the statistical uncertainties as additional information contained in the event sample is used. Since the cross section shows a much stronger residual scale dependence than the normalized distributions, the extended likelihood leads however to a significantly larger systematic uncertainty due to uncalculated higher order corrections. In addition, the uncertainty of the luminosity measurement which is not taken into account in the extended likelihood analysis leads to an additional uncertainty outweighing the gain in the reduced statistical uncertainty.

The estimators from the LO analyses on the other hand show a bias of $2.9 \times \Delta_{\text{stat}}$ and $38 \times \Delta_{\text{stat}}$ depending on whether the likelihood or the extended likelihood is used. It should be emphasized that the occurrence of a bias *per se*

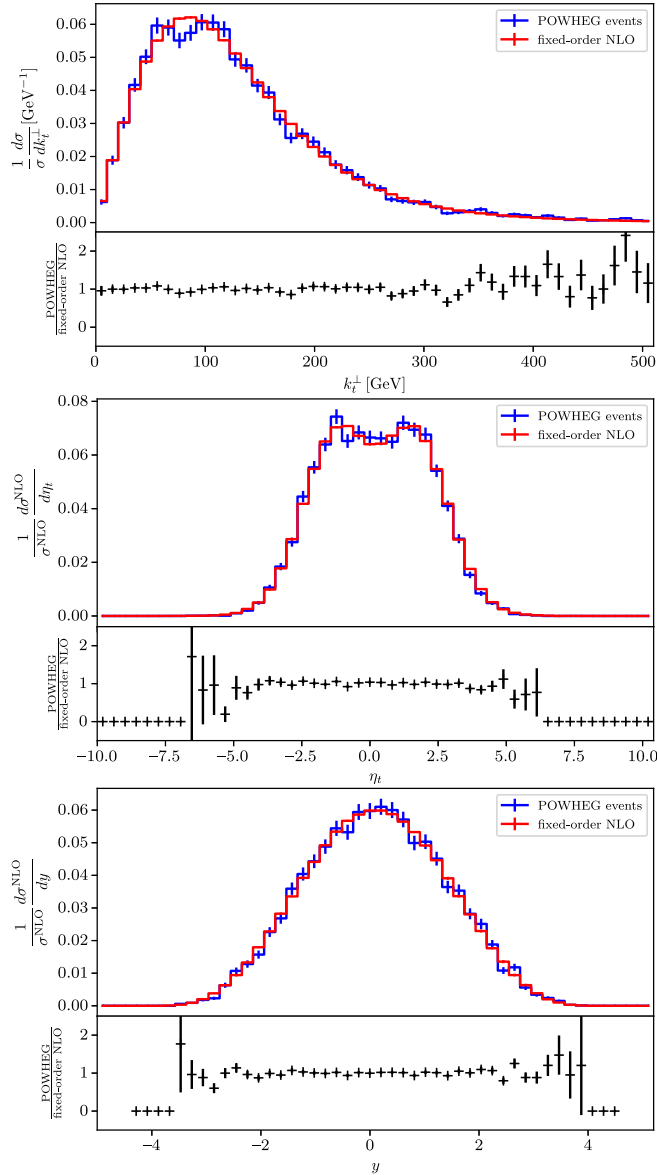


FIG. 7. Impact of the parton shower on the kinematic distributions of the top quark.

does not rule out the application of the MEM. It is well known, that the MEM typically leads to a bias if the probability distribution used in the evaluation of the likelihood does not match the distribution underlying the event sample. However, via a calibration procedure it is possible to compensate the bias and obtain an unbiased determination. Since the calibration can introduce additional uncertainties the preferred situation is that the probability distribution used in the likelihood determination matches the probability distribution of the event sample as best as possible thus reducing the need of additional calibration. As shown in Sec. II, the NLO corrections dominantly alter the normalization of the kinematic distributions rather than their shape. Accordingly, the analysis employing extended likelihoods which is sensitive to the total cross section shows thus a much stronger separation between the results obtained from the NLO and LO predictions.

Significant improvement from taking NLO corrections into account can be seen in their impact on the theoretical uncertainties; in the NLO analyses the theoretical uncertainties due to uncalculated higher order corrections are roughly halved with respect to the LO analyses.

In order to further study the robustness of the approach and having a more realistic simulation, unweighted events obtained from a parton shower simulation matched to the NLO calculation can be used. The parton shower resums certain logarithmic corrections to all orders on top of the fixed-order NLO parton-level calculation. Since these additional corrections present in the event sample are not accounted for in the fixed-order-only likelihood calculation based on Eq. (5), there is a mismatch between the underlying probability distribution of the generated events and the basis of the likelihood calculation [Eq. (5)]. As seen before in case of the LO analysis, this mismatch can cause a systematic bias in the extracted estimator.

Figure 7 shows the distributions obtained using POWHEG + Pythia [29–33] to generate about the same number of events as in the case of the fixed-order analysis. The parton shower only mildly affects the kinematic

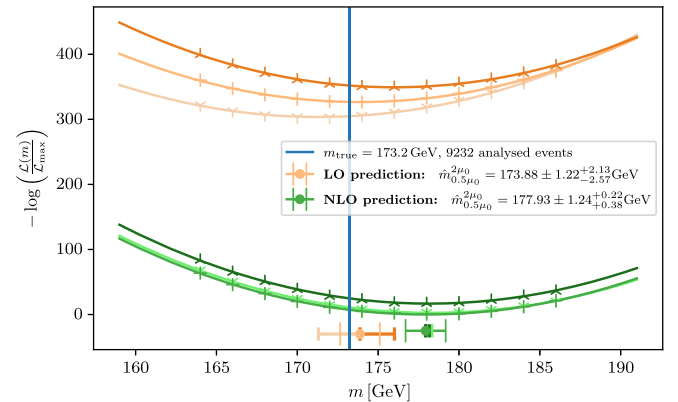


FIG. 8. Analysis of 9232 POWHEG + Pythia events with fixed-order likelihoods calculated at LO and NLO accuracy.

TABLE II. Extracted values for the estimator of the top-quark mass from unweighted POWHEG + Pythia events following the NLO prediction matched to a parton shower.

Likelihood	$\hat{m}_t \pm \Delta_{\text{stat}}^{\Delta_{\text{sys}}^{2\mu_0}} [\text{GeV}]$	
	LO prediction	NLO prediction
\mathcal{L}	$173.88 \pm 1.22_{-2.57}^{+2.13}$	$177.93 \pm 1.24_{+0.38}^{+0.22}$

distributions relevant for the event definition. Further distributions supporting this observation are shown in Fig. 13 in Appendix. Apart from minor differences in the k_T^\perp distribution at low k_T^\perp , a small difference is visible for $k_T^\perp > 300$ GeV, where the POWHEG + Pythia events lead to a slightly harder distribution than the events generated from the fixed-order NLO cross section.

The result of the likelihood analysis using LO and NLO cross section predictions is shown in Fig. 8 and summarized in Table II. We do not study the extended likelihood, since the extended likelihood leads to much larger systematic uncertainties. Again the statistical uncertainties are very similar for the LO and NLO analysis, while the systematic uncertainty is significantly reduced when using NLO predictions. In both cases we observe a shift of about 4 GeV compared to the results based on the event sample generated from the fixed-order NLO predictions. The large shift shows the high sensitivity of the MEM with respect to tiny changes in the distributions. In a mass determination from events registered at the LHC this shift must be taken into account via a calibration procedure. It is remarkable that the shift is, taking the uncertainties into account, independent from the perturbative order of the employed likelihood calculation. This is similar to what has been observed in Refs. [26,27]. The LO likelihood analysis reproduces the true mass value used in the POWHEG + Pythia analysis. However, this is most likely accidental and due to the fact that the LO fixed-order results undershoots the true mass value by about 4 GeV which is compensated by the aforementioned shift.

IV. CONCLUSION

In this work the MEM at NLO is applied to top-quark pair production at the LHC. To investigate the potential of the matrix element method to measure the top-quark mass, the MEM at NLO is applied to pseudodata; unweighted events generated from the fixed-order NLO cross section as well as events obtained using POWHEG + Pythia incorporating the parton shower effects. Using pseudodata based on POWHEG + Pythia allows to study the effect of the parton shower and gives a more realistic simulation. Including the NLO corrections in the likelihood calculation leads to a significant reduction of the theoretical uncertainties of the extracted top-quark mass, while the statistical uncertainties remain almost unchanged compared to the LO analysis.

We stress that the uncertainties due to scale variation cannot be reduced by a calibration. The reduction of the uncertainties associated with the scale variation when going from LO to NLO thus presents an important improvement and a strong argument in favor of the MEM at NLO accuracy.

Another important observation is the fact that the extended likelihood yields a significant improvement in terms of the statistical uncertainties. However, in practical applications this gain in precision is completely outweighed by the theoretical uncertainties of the number of expected events. This can be understood from the fact that, much as the NLO corrections (see Fig. 3), the scale variations do not dramatically change the shape of the kinematic distributions but mostly their normalization (see Fig. 4) thereby making the extended likelihood analyses more sensitive to their effect. Additionally, employing the extended likelihood requires precise knowledge of the integrated luminosity of the LHC. The dependence on this parameter introduces an additional source of systematic uncertainty. This has to be taken into account for future experimental applications of the MEM with realistic event numbers for abundantly produced top-quark pairs at the LHC which will most likely be dominated by systematic uncertainties. As has already been stated before in [25–28], for parameter inference with the MEM it is mandatory to perform the likelihood calculation at least at NLO accuracy in order to properly fix the renormalization scheme of the extracted parameter.

The application of the MEM at NLO to top-quark pair events at the LHC can offer an alternative approach to determine the top-quark mass with high accuracy. As has been demonstrated in this work, already for a few ten thousand events the precision of the analysis becomes dominated by systematic uncertainties. As the LHC produces millions of top-quark pairs, the analysis could be performed with a rather small fraction of cherry-picked events allowing to minimize the overall systematic uncertainty. The results obtained in this article suggest that top-quark mass determination with an uncertainty below 1 GeV could be feasible. Of course, for a realistic application of the MEM to experimental data, transfer functions accounting for decays, additional radiation and detector effects have to be considered. In addition, as the analysis based on the events including parton shower effects shows, a further calibration is required.

ACKNOWLEDGMENTS

This work was supported in part by the German Federal Ministry of Education and Research (Bundesministerium für Bildung und Forschung) under Contract No. 05H18KHCA1.

APPENDIX: ADDITIONAL RESULTS ON DISTRIBUTIONS USED FOR THE VALIDATION

In this appendix we show further cross checks used for the validation of the implementation. Figure 9

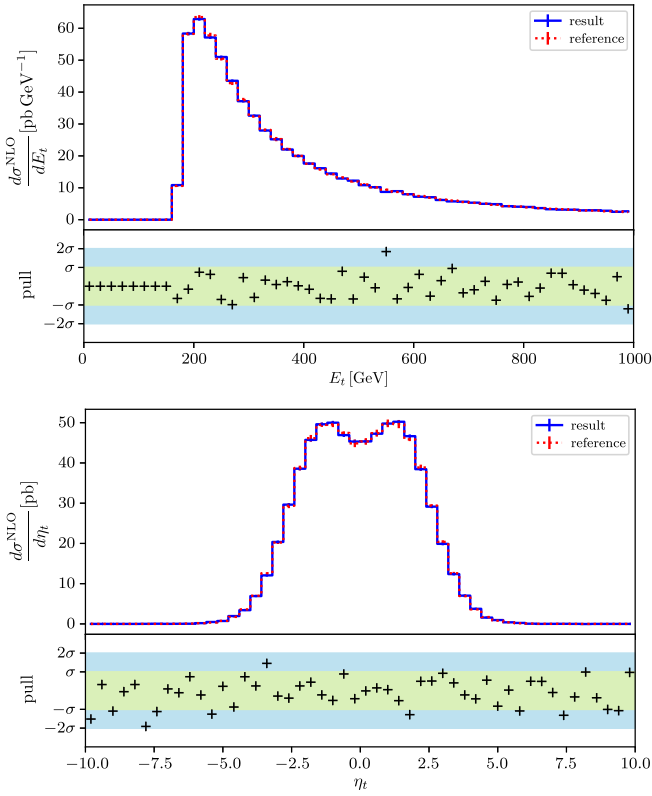


FIG. 9. Validation of the implementation: Comparison of differential distributions of the top quark obtained in this work with results from madgraph5 aMC@NLO.

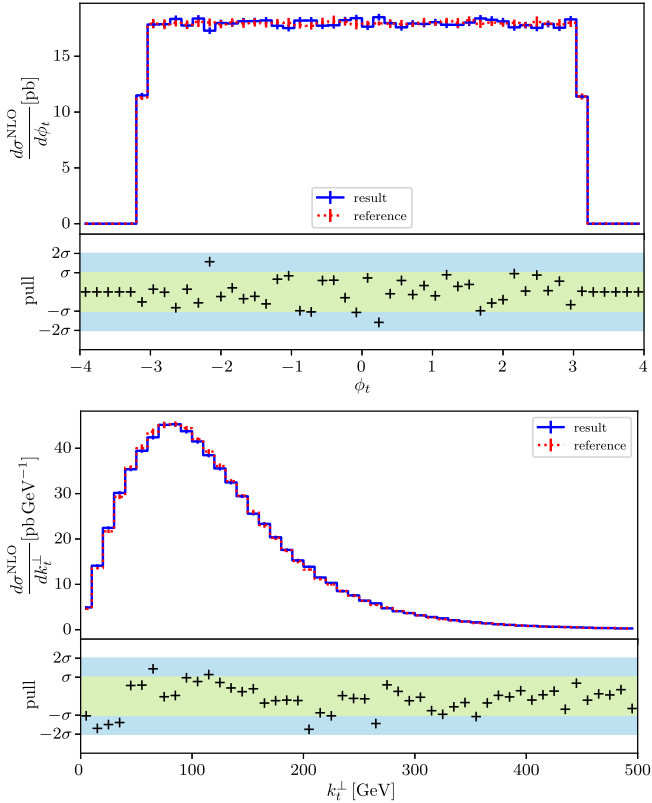


FIG. 10. Same as Fig. 9 but for the ϕ_t - and the k_t^\perp -distribution.

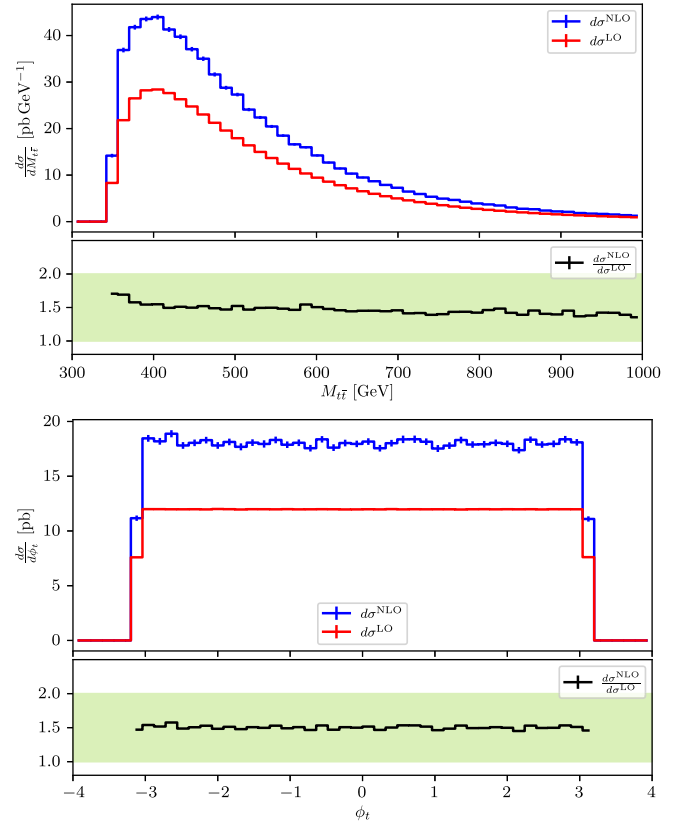


FIG. 11. Same as Fig. 3 but for the $M_{t\bar{t}}$ and the ϕ_t -distribution.

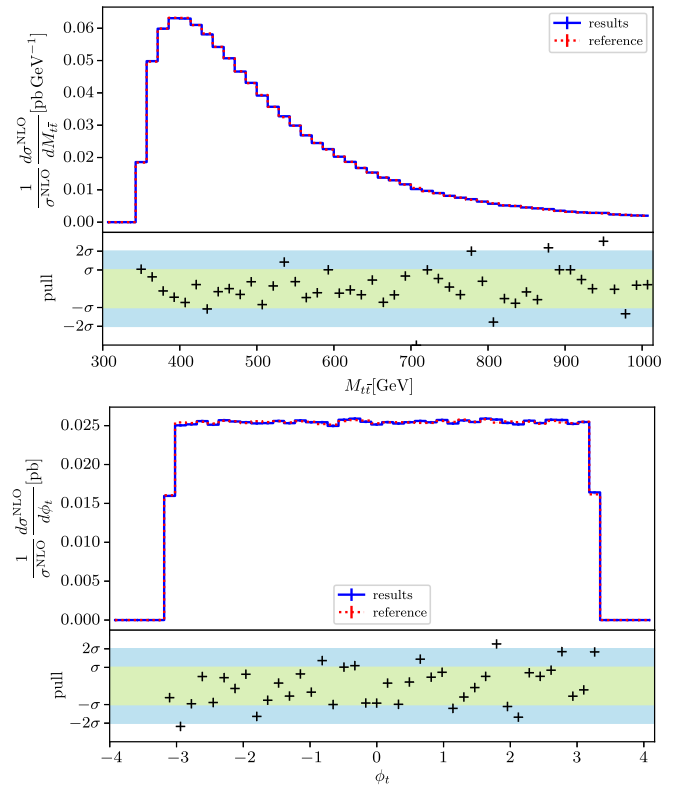


FIG. 12. Same as Fig. 5 but for the $M_{t\bar{t}}$ - and the ϕ_t -distribution.

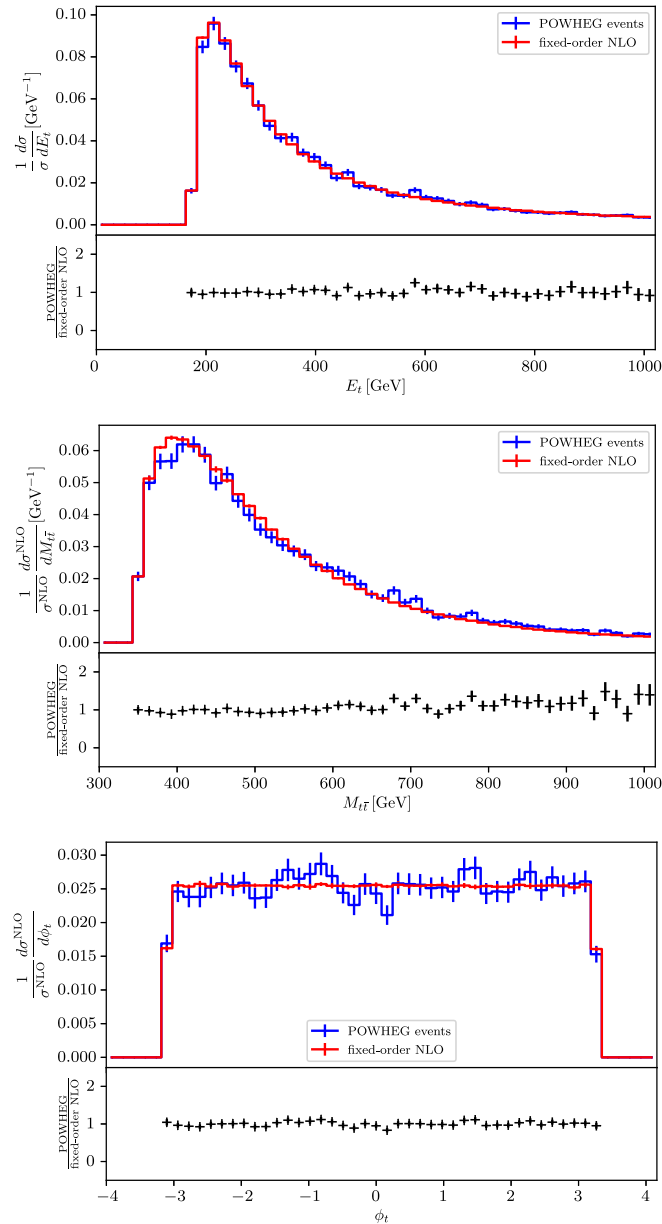


FIG. 13. Same as Fig. 7 but for the energy, $M_{t\bar{t}}$ - and ϕ_t -distribution.

shows comparisons of NLO predictions for differential distributions calculated in this work with distributions obtained from `madgraph5 aMC@NLO` [39] which is based on the dipole subtraction method [42,43]. The pull distributions in the bottom plots of Fig. 9 and Fig. 10 illustrate the agreement between both implementations within statistical uncertainties. This comparisons serve as a further validation for the choice of the slicing parameter. Figure 11 shows the NLO corrections (upper part) together with the

k -factors (lower part) for the $M_{t\bar{t}}$ and the ϕ_t -distribution. Similar to what is shown in Fig. 3, a flat k -factor is observed again. As a check of the event generation and the unweighting procedure Fig. 12 shows distributions calculated from the generated unweighted events compared with a calculation using `madgraph5 aMC@NLO` [39]. Similar to Fig. 7 we show in Fig. 13 for further distributions the comparison of distributions obtained at fixed-order NLO accuracy with results using POWHEG + Pythia.

- [1] P. Nason, S. Dawson, and R. K. Ellis, *Nucl. Phys.* **B303**, 607 (1988).
- [2] P. Nason, S. Dawson, and R. K. Ellis, *Nucl. Phys.* **B327**, 49 (1989); **B335**, 260(E) (1990).
- [3] W. Beenakker, H. Kuijf, W. L. van Neerven, and J. Smith, *Phys. Rev. D* **40**, 54 (1989).
- [4] W. Beenakker, W. L. van Neerven, R. Meng, G. A. Schuler, and J. Smith, *Nucl. Phys.* **B351**, 507 (1991).
- [5] W. Bernreuther, A. Brandenburg, Z. G. Si, and P. Uwer, *Nucl. Phys.* **B690**, 81 (2004).
- [6] K. Melnikov and M. Schulze, *J. High Energy Phys.* **08** (2009) 049.
- [7] M. Czakon, P. Fiedler, and A. Mitov, *Phys. Rev. Lett.* **110**, 252004 (2013).
- [8] M. Czakon, D. Heymes, and A. Mitov, *Phys. Rev. Lett.* **116**, 082003 (2016).
- [9] M. Czakon, P. Fiedler, D. Heymes, and A. Mitov, *J. High Energy Phys.* **05** (2016) 034.
- [10] S. Catani, S. Devoto, M. Grazzini, S. Kallweit, J. Mazzitelli, and H. Sargsyan, *Phys. Rev. D* **99**, 051501 (2019).
- [11] S. Catani, S. Devoto, M. Grazzini, S. Kallweit, and J. Mazzitelli, *J. High Energy Phys.* **07** (2019) 100.
- [12] M. Beneke, M. Czakon, P. Falgari, A. Mitov, and C. Schwinn, *Phys. Lett. B* **690**, 483 (2010).
- [13] M. Czakon, A. Mitov, and G. F. Sterman, *Phys. Rev. D* **80**, 074017 (2009).
- [14] M. Beneke, P. Falgari, S. Klein, and C. Schwinn, *Nucl. Phys.* **B855**, 695 (2012).
- [15] M. Cacciari, M. Czakon, M. Mangano, A. Mitov, and P. Nason, *Phys. Lett. B* **710**, 612 (2012).
- [16] N. Kidonakis, *Phys. Part. Nucl.* **45**, 714 (2014).
- [17] A. Ferroglia, B. D. Pecjak, and L. L. Yang, *Phys. Rev. D* **86**, 034010 (2012).
- [18] A. Ferroglia, S. Marzani, B. D. Pecjak, and L. L. Yang, *J. High Energy Phys.* **01** (2014) 028.
- [19] M. Czakon, A. Ferroglia, D. Heymes, A. Mitov, B. D. Pecjak, D. J. Scott, X. Wang, and L. L. Yang, *J. High Energy Phys.* **05** (2018) 149.
- [20] W. Beenakker, A. Denner, W. Hollik, R. Mertig, T. Sack, and D. Wackerroth, *Nucl. Phys.* **B411**, 343 (1994).
- [21] W. Bernreuther, M. Fuecker, and Z.-G. Si, *Phys. Rev. D* **74**, 113005 (2006).
- [22] J. H. Kühn, A. Scharf, and P. Uwer, *Eur. Phys. J. C* **51**, 37 (2007).
- [23] S. Moretti, M. R. Nolten, and D. A. Ross, *Phys. Lett. B* **639**, 513 (2006); **660**, 607(E) (2008).
- [24] D. Pagani, I. Tsinikos, and M. Zaro, *Eur. Phys. J. C* **76**, 479 (2016).
- [25] T. Martini and P. Uwer, *J. High Energy Phys.* **09** (2015) 083.
- [26] T. Martini and P. Uwer, *J. High Energy Phys.* **05** (2018) 141.
- [27] M. Kraus, T. Martini, and P. Uwer, *Phys. Rev. D* **100**, 076010 (2019).
- [28] M. Kraus, T. Martini, S. Peitzsch, and P. Uwer, *arXiv*: 1908.09100.
- [29] P. Nason, *J. High Energy Phys.* **11** (2004) 040.
- [30] T. Sjostrand, S. Mrenna, and P. Z. Skands, *J. High Energy Phys.* **05** (2006) 026.
- [31] S. Frixione, P. Nason, and C. Oleari, *J. High Energy Phys.* **11** (2007) 070.
- [32] S. Frixione, P. Nason, and G. Ridolfi, *J. High Energy Phys.* **09** (2007) 126.
- [33] S. Alioli, P. Nason, C. Oleari, and E. Re, *J. High Energy Phys.* **06** (2010) 043.
- [34] W. T. Giele, E. W. N. Glover, and D. A. Kosower, *Nucl. Phys.* **B403**, 633 (1993).
- [35] S. Badger, R. Sattler, and V. Yundin, *Phys. Rev. D* **83**, 074020 (2011).
- [36] T. Kinoshita, *J. Math. Phys. (N.Y.)* **3**, 650 (1962).
- [37] T. D. Lee and M. Nauenberg, *Phys. Rev.* **133**, B1549 (1964).
- [38] M. Aliev, H. Lacker, U. Langenfeld, S. Moch, P. Uwer, and M. Wiedermann, *Comput. Phys. Commun.* **182**, 1034 (2011).
- [39] J. Alwall, R. Frederix, S. Frixione, V. Hirschi, F. Maltoni, O. Mattelaer, H. S. Shao, T. Stelzer, P. Torrielli, and M. Zaro, *J. High Energy Phys.* **07** (2014) 079.
- [40] J. von Neumann, in *Monte Carlo Method*, National Bureau of Standards Applied Mathematics Series Vol. 12, edited by A. S. Householder, G. E. Forsythe, and H. H. Germond (US Government Printing Office, Washington, DC, 1951), Chap. 13, pp. 36–38.
- [41] A. Butter, T. Heimel, T. Martini, S. Peitzsch, and T. Plehn, *arXiv*:2210.00019.
- [42] S. Catani and M. Seymour, *Nucl. Phys.* **B485**, 291 (1997).
- [43] S. Catani, S. Dittmaier, M. H. Seymour, and Z. Trocsanyi, *Nucl. Phys.* **B627**, 189 (2002).